Title

Liquid transmission characteristics of padding bandages under pressure

Journal

Journal of Biomaterials Applications, 30(5)

ISSN

0885-3282

Authors

Kumar, Bipin

Das, Apurba

Pan, Ning

et al.

Publication Date

2015-11-01

DOI

10.1177/0885328215597589

Peer reviewed

Liquid Transmission Characteristics of Padding Bandages under Pressure

[*,1]Bipin Kumar, [2]Apurba Das, [1]Ning Pan, [2]R. Alagirusamy, [2]Rupali Gupta and [2]Jitender Singh

[1]Textiles and Clothing, UC Davis, CA, USA 95616

[2]Department of Textile Technology, IIT Delhi, Delhi, India, 110016

Abstract

Padding is an essential component in a multilayer compression bandaging system, used inside the compression bandage through which substantial amount of pressure is exerted on the limb of patient for treatment of venous leg ulcers. As a result, the liquid transmission behavior of padding is also critical in managing body fluids or sweat exuded from the affected limb, reducing the excessive moisture build-up around the wound and thereby ensuring comfort to and hence a better compliance from the patients. This study investigates the in-plane fluid transport characteristics of needle-punched nonwoven padding bandages. It first reviewed the existing studies related to the problems, and discussed their limits and possible improvements in dealing with complex fluid transport issues in textile porous media. The measurement of fluid transport under different pressure levels was then done using a newly designed apparatus capable of simultaneously tracing the liquid in-plane spreading along different directions, and obtaining several transport characteristics of a testing sample, e.g., the liquid flow anisotropy, the rate of movement, the area of wet surface with time, etc. Also the effects of several important factors, such as the levels of pressure applied, the specimen bulk density and needling density of the padding products, have been experimentally investigated.

In addition, based on an extended Lucas–Washburn theory, we calculated the liquid flow distance, both instantaneous speed and a more useful time-averaged speed v_{av} at any given direction, and

also defined a flow anisotropy index I_A as a convenient parameter to represent the material flow anisotropy. The applications of v_{av} and I_A to actual samples have demonstrated the usefulness of these parameters in characterizing the flow nature and behavior of the materials.

Keywords: Padding, liquid transport, normal pressure, compression therapy, multi-layer bandaging system, nonwovens

Short Title: Wicking of padding for wound care management

* Address for correspondence. Dr. Bipin Kumar, Postdoc Scholar, Textile and Clothing, UC Davis, CA, 95616, Unites States. E-mail address: bipiniitd18@gmail.com

1. Introduction

The physico-mechanical properties of porous fibrous materials are important in assessing their performance in several medical/biomedical applications such as, absorbance pads, padding bandages, wound dressings, diapers, protective medical underwear, etc (1-4). One of such properties is the liquid management of padding bandages used in compression therapy - the single most effective means in treatment of chronic venous and lymphatic insufficiencies (5, 6). Padding and compression bandages are both utilized in two or multilayer compression bandaging systems recommended for compression treatment (7-9), with padding bandage as the innermost layer in contact with skin. Padding plays a critical role in the successful treatment of venous leg ulcers by ensuring uniform pressure distribution beneath the bandaging layer around the circumference of leg (2). Apart from the pressure management, paddings also facilitate body fluid absorption and removal for comfort and better patient-compliance of the multi-layer compression systems (9), as the padding bandage is frequently in interaction with body fluids or exudate, in addition to sweat. As the whole compression system is usually worn for a prolonged time with a low frequency of dressing changes (10), and body fluids should hence be effectively removed from the affected wound portion to prevent moisture build-up and condensation (11), causing over hydration and even maceration of the tissues (12). The liquid transport or wicking of the padding is thus critical as it determines the ability of the padding to spread the body fluid to a wider area for quicker evaporation so as to prevent excessive moisture build-up (4). All the above facts highlight the importance of wicking (liquid transport) behavior of a padding and demand for its detailed examination. This would improve the understanding of the compression treatment and assist in evaluation and design so as to provide optimized product for comfort and better compliance from the patients.

Non-woven structure made from polyester, viscose or polypropylene fibers are primarily used as padding materials (2). A needle-punched nonwoven is a complex three dimensional porous network of fibrous materials, resulted from mechanical interlocking by the action of needle punching (13). Its liquid transport capacity is primarily determined by the porous structure for transmission of liquid in the network via the capillary force (14), and the structure is in turn decided by the fibers and the processing parameters, e.g., fiber size and distribution, depth of needle penetration, amount of feed, needle punching frequency, etc. These parameters should be taken into consideration in evaluating wicking performance of the padding bandages.

Padding bandage lies underneath the compression bandage that applies significant amount of interface pressure in the range from 10 to 50 mmHg to the leg (15), depending of severity of venous disease (16). Under external compression, the porosity or indeed the wicking performance of the padding will change significantly; so it is expected that the liquid transmission behavior of the same padding material will vary when exposed to different levels of normal compression. Clearly, the effect of the external pressure has to be accounted for in the analysis. The purpose of this research is to provide more detailed descriptions of the in-plane liquid transport characteristics of padding, including the influences by such factors as bulk density, needling density and normal pressure.

2. Theoretical Framework

The basic theory in the field of nonhomogeneous flows was proposed by Young and Laplace in the form of capillarity equation (14, 17, 18):

$$\Delta P = 2\gamma H = \gamma\left(\frac{1}{R_1}+\frac{1}{R_2}\right) \quad (1)$$

ΔP is the pressure difference across the fluid interface, γ is the surface tension (or wall tension) and H is the mean curvature of the surface, and R_1 and R_2 are the principal radii of the curvature. This describes the capillary pressure difference sustained across a curved interface between two immiscible fluids, such as water and air, due to the phenomenon of surface or wall tension and the liquid flow starts once the actual pressure difference is greater than ΔP . Lucas and Washburn further extended their work on capillary-driven nonhomogeneous flows and developed what is known as the Lucas–Washburn theory that has been frequently used in textile areas (14, 17, 19, 20). For a cylindrical capillary tube with a constant radius *r* in which a liquid has flowed along the capillary axis a distance *l*, this theory can be expressed into (17, 19)

$$\frac{dl}{dt} = \frac{r\gamma\cos\theta}{4\mu l} - \frac{r^2\sigma g\cos\beta}{8\mu} \tag{2}$$

Where, σ is the density, μ the viscosity, and γ the surface tension of the liquid; g is the gravitational acceleration; θ the contact angle between the liquid surface and the capillary wall, and β denotes the angle between the tube and the vertical axis. As the parameters, *r, γ, θ, μ, σ, g* and β remain constant for a given system, so the instantaneous flow speed in Eq. 2 can be simplified to:

$$\frac{dl}{dt} = \frac{A}{l} - B \tag{3}$$

Where, *A* and *B* are constants. Eq. 3 indicates that in an erected capillary tube with angle β, the liquid climbing rate decreases with the climbing height. Note that like in several other basic equations (e.g. Fourier Law in heat conduction), Eq. 3 also implies an infinite climbing rate in the beginning when $l = 0$, which is of course not physically possible. It is nevertheless useful in

studying general capillary flow problems. When the penetration of liquid is horizontal ($\beta = 90^{\circ}$), the effects of the gravitation field are negligible and the acceleration g in Eq. 2, and hence the term B in Eq. 3 vanish. The wicking length l can be solved as (17, 19):

$$l = \sqrt{2At} \tag{4}$$

The above equation can be used to guide our experimental study in next section where the liquid is poured in at the center of a thin textile substrate and spreads radially outward in the horizontal plane. However two issues have to be mentioned: first, as the textile substrate is structurally anisotropy, one has to expresses the capillary radius r and therefore the wicking length l both as functions of the flow direction, say α. More important, Eq. 4 is derived for a single uniform capillary radius r. When applied to a porous medium like fabric, local r values fluctuate not only between the different direction, but also along the same direction. So a comprehensive effective capillary radius r_α has to be used which would generate, at the macro-level, the equivalent kind of flow as in the original porous material, turning the constant A into a function of direction, *i.e.,* $A = A_\alpha$. Then the total travel length at any given direction after a total travel time T:

$$R = \sqrt{2A_\alpha T} \tag{4b}$$

As the specimen is a circle and let the flow reaches the specimen fringe, $R = R_o$ will be a constant. But at different flow direction α, the total travel time $T = T_\alpha$ will attain different values, i.e.,

$$T_\alpha = \frac{R_o^{\,2}}{2A_\alpha} \tag{5}$$

Then among the T_α values at different directions for the same specimen, we can use the ratio,

$$I_A = \frac{T_{\alpha\,min}}{T_{\alpha\,max}}, \qquad 0 < I_A < 1 \tag{6}$$

as a convenient index to reflect the degree of flow anisotropy, and a smaller I_A value represents a more anisotropic material, where the subscripts *αmin* and *αmax* correspond to the directions where the total travel time T_α acquires its minimum and maximum values, respectively. The actual total travel time T_α in other directions will be within them, i.e., $T_{\alpha\,min} \le T_a \le T_{\alpha\,max}$, and the equal sign in both indicates an isotropic specimen.

As an in-plane case, the flow speed in Eq. 3 now reduced to,

$$\frac{dl}{dt} = \frac{A_\alpha}{l} \tag{3b}$$

but is still a function of both wetting distance l and time t, not convenient to use in comparing different specimens. We hence define a time-averaged flow speed using the ratio of the total travel length and total travel time in any given direction α, i.e.,

$$v_{av} = \frac{R_o}{T_\alpha} = \frac{R_o}{R_o^{\,2}} \times 2A_\alpha = \frac{2A_\alpha}{R_o} = \frac{r_\alpha \gamma \cos\theta}{2\mu R_o} \tag{7}$$

As the parameters γ, θ, μ and R_o are fixed, this average velocity v_{av} depends only on the effective radius of capillary r_α in the flow direction α. More practically, once the coefficient A_α is given, the v_{av} value at the direction can be easily calculated.

3. Material and Methods

3.1. Padding materials

The process of needle punching is one of the production methods for nonwovens where the fibrous network is formed by mechanical interlocking that is achieved with thousands of barbed felting needles repeatedly passing into and out of a fibrous web (13). In this study, a series of 12 padding samples (sample codes A1 to A9) was prepared using needle-punched nonwovens manufactured using a DILO needle-punched machine that consists of an opener, card, cross lapper and needle loom. The fibers are 6-denier polypropylene staple of cylindrical shape. The layering factor and output of the card were adjusted to achieve the required mass per unit area, while the punching frequency of needle board was varied to change the needling density of the products. All the nonwovens were punched with the Groz Beckert needle which has the specification of R332 G53012. The depth of needle penetration during the production was kept constant (0.01 m) for all paddings. Table 1 shows the main characteristics of these padding samples, with mass per unit area varies from 100 to 300 g/m^2, and needling density ranges from 50E4 to 210E4 punches/m^2.

Table 1: Details of the paddings

Sample code	Fiber	Fiber linear density, (denier)	Areal density, S_o (g/m^2)	Needling density, x10^4 (punches/m^2)	Thickness, t_o (mm)	Density $\rho_{so} = S_o / t_o$ (g/m^3) x10^3	Pore volume fraction (ε_o)
A1	PP	6	100	50	4.75	21.05	97.77
A2	PP	6	100	130	4.12	24.27	97.43

A3	PP	6	100	210	3.79	26.39	97.21
A4	PP	6	200	50	5.34	37.45	96.04
A5	PP	6	200	130	4.97	40.24	95.75
A6	PP	6	200	210	4.54	44.05	95.34
A7	PP	6	300	50	6.02	49.83	94.73
A8	PP	6	300	130	5.74	52.26	94.48
A9	PP	6	300	210	4.74	63.29	93.31

Note: PP – polypropylene

3.2. Measurement of liquid transmission in the paddings

As mentioned above, the liquid transmission in the plane of padding is more relevant for our case as the thickness of the padding is tiny relative to other dimensions. Next to the impractical practice of examining the padding materials performance on a human subject, instrumental approach to measure the liquid transmission behavior of the material under controlled conditions is a useful tool to obtain non-biased results for fair evaluation of different padding samples. Several experimental techniques have been developed for evaluating fluid transport behavior in fibrous materials, including image analysis technique, electrical methods, weighing method, etc. (21-25). However, none of the existing methods is able to conduct measurement while the sample is under external pressure as padding bandage is when in use. As such compression will significantly distort the original padding internal structures and thus alter the liquid wetting behavior, it is therefore essential to develop a suitable experimental set-up capable of applying pressure and simultaneously observe/record the liquid flow in padding

nonwovens. Also, given the anisotropic nature of porous media, it is important to capture the direction dependence of the flow behaviors.

Accordingly we designed a new-experimental set-up for the wicking measurement. The prototype is based on a capacitive principle that the capacitance of a parallel plate capacitor varies with changing of the dielectric medium between the parallel plates (26, 27), i.e.,

$$C = \frac{k\varepsilon_o A}{d} \tag{8}$$

where, C is the capacitance, k is the relative permittivity of the dielectric material between the plates, ε_o is vacuum permittivity (8.854E-12 F/m), A is the area of the each plate and d is the distance between the plates. Dielectric constant is an inherent characteristic of a particular material; for example, water has a k value of 80.10 at 20ºC, while a fibrous sheet has a different dielectric constant depending on its composition. Therefore, a fibrous assembly in dry and wet conditions will have dissimilar dielectric constants. If the liquid flows through a padding placed between the capacitor plates, then the capacitance of the system will change according to the amount of the liquid or the variation in the overall effective dielectric constant of the padding. This change in capacitance can be recorded, and used to derive several parameters related to the liquid transport, i.e., rate of transport, extent of liquid spreading in different directions, area of wet surface with time, etc.

3.2.1. Instrumental set-up

The set-up consists of two circular discs (upper and lower) made of Polyamide (Commercial name PA2200) with the same dimensions (radius of each disc = 0.12 m), and on each disc, eight slots are grooved along the radius and each filled with a copper strip

symmetrically arranged at a 45º spacing angle to cover the disc (Figure 1a). So once a circular padding specimen as the dielectric medium (thickness = 0.04 m, diameter = 0.11 m) is placed in between the two discs, 8 equivalent capacitors are formed with two upper and lower copper strips as the electrodes, and adhesive PVC insulation tape is used to prevent undesirable electric discharges. Any change in capacitance caused by water flowing will be sensed and delivered to the instrument via the wiring on the electrodes so as to obtain water flow behavior along different directions through the padding. Figure 1a shows the photograph of the apparatus. The liquid is discharged from a burette via a flow tube to a small orifice that is located at the center of the upper disc. The flow tube is fitted with an IV-drip system which helps maintain a constant flow rate throughout the study.

Insert Figure 1

3.2.2. Measurement of wicking distance (*l*)

Once a padding specimen is placed between the discs, and liquid is poured at the center, the liquid flows in the plane of the specimen due to the capillary action (Figure 1b), and the system consists of wet and dry parts of the specimen that act as different dielectric materials between the capacitor plates. During the liquid spreading, the capacitance of each individual capacitor in a given direction changes continuously, and is recorded using a data acquisition system with the instrument. These capacitance readings can be used to measure the distance travelled by the water at any particular instant in the specimen along 8 different directions as shown in Figure 1b. The distance *l* travelled by the liquid in a particular direction and instant can be calculated as,

$$l = \frac{C_x - C_{dry}}{C_{wet} - C_{dry}} \times R \quad (9)$$

where, R = 11 cm is the radius of the specimen, , C_{dry} is capacitance of the system when the specimen is completely dry, C_{wet} capacitance of the system when the specimen is completely wet (i.e., liquid spread out to full length), C_x is the capacitance of the system at a particular instant when water travelled a radial distance l. More details were provided by Kumar and Das, 2013 (26, 27).

3.2.3. Measurement under normal pressure

The properties of the padding specimen, e.g., specimen thickness, pore dimensions, and hence the liquid flow behaviors, will be altered once a pressure is applied on it. To evaluate the effect, external pressures are applied to the upper disc by placing standard weights. In the beginning, test is done at a normal pressure of 0.2 kPa (P_o) which is the pressure applied by the upper disc alone on the specimen. Three more pressure levels of 0.8, 1.5 and 2 kPa can be applied subsequently on the testing specimens using different weights. These weights are circular in shape in order to distribute the normal pressure uniformly on the specimen.

3.3. Design of experiment

For the test specimens, four levels of mass per unit area (100, 200 and 300 g/m^2) and three levels of needling density (50, 130 and 210 x10^4 punches/m^2) were used to examine their effects on the water transmission. Moreover, the liquid flow behaviors under four levels of normal pressures (0.2, 0.8, 1.5 and 2 kPa) were tested as discussed above. Distilled water was used as the liquid with a discharging rate kept constant (0.125 cc/s) for each test. For each individual test, the machine direction of the specimen was aligned in the same direction, i.e., α1,

Deleted:

in the instrument while measuring. The whole testing procedure was carefully checked and the sensitivity in the capacitance measurement is ± 0.1 picofarad. Several initial trails were done for the calibration of the apparatus prior to the actual tests. For each sample, 5 repeated tests were performed using individual specimens, and the average value is calculated and used in analysis. For the comparison, ANOVA (analysis of variance) analysis was performed to determine whether there were any significant errors in the mean values at different levels of conditions, and a p-value less than 0.05 was considered as statistically significant.

4. Results and discussion

4.1. Nature of in-plane liquid flow

The proposed apparatus is useful to obtain several important parameters related to wicking, e.g., the extent of water flow in different directions or the uniformity of water spreading (flow anisotropy), rate of flow, area of wet surface with time, etc. Table 2 shows the recorded liquid flow along 8 different directions α_1 to α_8 for padding A2 at pressure P = 0.2 kPa. As seen from the data, once the liquid (water) is discharged at a constant rate at the center of the specimen, it starts spreading radially, covers 5.76 cm (~ 50% of the total length) in direction α_1 in 300 s (5 min), and reaches to the end in nearly 15 min, viz. the rate of spreading is very high in the beginning, and reduces with time. If we plot the wetting length l versus time using Eq. 4 $l = \sqrt{2A_\alpha t}$, where A_α is a function of, among other things, the flow direction α and can be estimated from the experimental results. For instance, the A_α value for this case in direction α_1 is 0.063 via the regression analysis. Using A_α value in Eq. 4 for the wetting distance l and flow velocity $v = dl/dt$ (i.e., the instantaneous rate of spreading), both being functions of time t, we

compared our experimental data in Table 2 with the predictions for sample A2 along direction α_1 in Fig. 2 for l and v, respectively. At the beginning, the liquid spreads and occupies the free space available in the pores of the specimen and the air in the pores presents little resistance to the flow, thus the faster spreading. Once those capillaries become more saturated, and less easily accessible space is available, leading to a higher resistance or a decreasing v. As v is a valuable indicator of the padding response, but is changing with time, we calculated, using Eq. 7, the average value v_{av} over the entire flow period and use it as a liquid flow parameter along the given direction of the specimen.

Insert Figure 2

Again if we can derive the complete expression for coefficient A_α to include the directional information, Eq. 4 can be used to describe the non-uniform flow of fluid in different directions (α_1 to α_8) as reflected by the experimental data in Table 2. For illustration, the values of A_α in Eq. 4 are estimated from the data in the table for sample A2, as 0.063, 0.082, 0.077, 0.072, 0.071, 0.064, 0.074 and 0.075 cm^2/s respectively at directions α_1 to α_8. The total traveling time T_α in each direction, are also provided in Table 2. It is clear from the data in Table 2 that even though the samples are all non-woven, thus having fewer variations at different directions than other textile fabrics, the flow anisotropy is still clearly exhibited, judging from either the coefficient A_α or the total traveling time T_α.

Table 2: Results of radial spreading in different directions for Specimen A2 (P = 0.2 kPa)

Time,	**Radial distance *l* travelled in different directions (α_1 to α_8), cm**							
(s)	α_1	α_2	α_3	α_4	α_5	α_6	α_7	α_8
0	0.00	0.00	0.00	0.00	0.00	0.00	0.00	0.00
20	0.56	2.75	1.59	1.76	0.55	0.44	1.26	2.87
40	1.03	3.92	2.52	2.62	1.25	1.15	2.22	3.61
60	1.48	4.43	3.43	3.26	1.94	1.99	3.45	4.50
120	2.72	6.25	5.18	4.93	4.09	3.33	5.88	5.87
200	4.25	8.34	7.40	6.66	5.64	5.30	7.86	7.24
300	5.76	9.32	8.47	7.75	7.26	6.55	8.41	8.38
400	6.84	9.64	9.25	8.53	8.38	7.17	8.62	9.01
600	8.51	10.17	10.01	9.49	9.32	8.38	9.33	9.55
800	10.11	10.80	10.51	10.25	10.50	9.99	10.42	10.25
Total time, T_α (s)	895	837	870	886	865	884	855	873

Of course another important issue is the comparison between 9 different padding materials shown in Table 1 in their transport behaviors. Based on T_α values obtained at 8 different directions for each of the 9 products, and we calculated the anisotropic index I_A using Eq. 6 for every product, as in Table 3. First, it is clear what we discussed about the flow anisotropy for A2 in Table 2 is true for other samples, as judging from the directional variations of the total traveling time T_α in each sample. However such discrepancies in T_α within each

sample are not very large, again the reflection of the relative structural uniformity in non-woven materials. Of all 9 samples, the minimum I_A value for A1 is still 0.87, not too far from 1.

Although I_A offers a convenient and comprehensive description of a sample flow anisotropy, its definition reveals that it is not sensitive to the specific flow details. For instance, let's compare Samples A1 and A9, both showing very close I_A values, A1 (0.87) and A9 (0.88), and hence is very similar in terms of overall flow anisotropy. However the two specimens are at extremes in terms of the fiber volume fraction, A1 (2.23%) and A9 (6.69%), resulted mainly from the increased needling density from A1 (50) to A9 (210). The differences in these parameters resulted in a very different flow process between them; the much open and porous structure in A1 led to a much fast flow rate (much shorter T_α) at all directions, as clearly exhibited in Table 3. So in other words, T_α is useful to illustrate the difference within a sample between different directions, where as I_A is more suitable to make an overall comparison between samples.

Table 3: Result of the flow anisotropy behavior for different samples (P = 0.2 kPa)

Sample	**Total Traveling Time in different directions, T_α (s)**								$I_A = \frac{T_{\alpha\ min}}{T_{\alpha\ max}}$
	α_1	α_2	α_3	α_4	α_5	α_6	α_7	α_8	
A1	477	495	452	454	444	487	433	481	0.87
A2	895	837	870	886	865	884	855	873	0.93
A3	1155	1109	1076	1023	1107	1091	1141	1102	0.88
A4	598	564	581	596	621	605	573	615	0.91
A5	1050	1078	1144	1063	1109	1097	1083	1134	0.92
A6	1435	1523	1376	1476	1446	1505	1427	1520	0.90

A7	735	705	643	697	723	681	655	708	0.89
A8	1215	1232	1164	1197	1205	1261	1155	1145	0.91
A9	2210	2029	2113	2095	2035	2289	2176	2067	0.88

On the other hand, if just looking at the data in the table, comparison between A3 and A5 is not as straight forward, although both samples are different in nearly every parameter, including the fiber volume fraction, A3 (2.79%) and A5 (4.25%), and the I_A ranking in ascending order is A3 = 8 and A5 = 2. We hence constructed a spider-web chart as in Fig. 3 using the T_α values in each direction for the two samples, and it enables a more comprehensive and easy examination. For instance, it shows that both samples maintain a nearly identical flow rate at directions α_5 and α_6, but different flow speeds in all other directions. A3 achieved the highest speed in direction α_4 whereas A5 in direction α_1.

Insert Figure 3

4.2. Effect of normal pressure

Theoretical prediction of the influence on the flow behavior by such related parameters as the normal pressure applied, the sample bulk density and the needling density, can be accomplished if those factors can be explicitly included in the expression for the comprehensive effective capillary radius r_α in Eq. 2. However we have to leave it to future study and resort to the experimental data here. Fig. 4 shows the average flow speed v_{av} at different levels of

pressure, i.e., 0.2, 0.8, 1.5 and 2 kPa, measured for Sample A1. As there are 8 directions in one sample and each corresponds to a different v_{av} value, for simplicity, we only compare the maximum v_{av} values, regardless the associated directions, at the 4 pressure levels. From the experimental data, v_{av} decreases with increasing pressure, with faster drop initially. However, with further increase in pressure, the reduction rate slows down, and v_{av} then reaches a saturation point at high pressure (2 kPa). Increasing normal pressure on a padding specimen impedes the capillaries, and decreases the pores size or the porosity of the fibrous structure significantly. It causes more drag or resistance to the liquid movement through the network, and hence the reduction in flow speed.

Insert Figure 4

4.3. Effect of initial specimen areal density S_o

The initial areal density S_o is a very important material property used extensively in practical applications. In order to examine its effect experimentally, we have to compare samples among which the only difference is in S_o. We first selected Samples A1, A4 and A7 who are otherwise identical in all parameter, except S_o plus, unfortunately, the initial thickness t_o. To overcome that, we use the sample initial density ρ_{so} values provided in Table 1, where $\rho_{so} = S_o / t_o$. This way the three samples only differ in ρ_{so} values: A1 (21.05E3 g/m^3), A4 (37.45E3 g/m^3) and A7 (49.83E3 g/m^3). Note that there is

$$\frac{\rho_s}{\rho_f} = 1 - \varepsilon \qquad (10)$$

Where ρ_f is the fiber density and ε is the sample porosity. Fig. 5 exhibits the effect of sample density on v_{av}, again under increasing pressure for all 3 samples A1, A4 and A7. As the only difference among the 3 samples is in the sample initial density ρ_{so}, so whatever discrepancies between the 3 curves can only be attributed to ρ_{so}. As expected, at a given pressure level, a higher density ρ_{so} value, i.e., more fibers in a given volume, indicates a smaller effective capillary radius r, leading to a decreasing average flow speed v_{av}. If you further examine the percentage change in v_{av} values, the pressure effect appears to be more pronounced for higher density samples. For instance, when pressure increase from 0.2 to 2 kPa, v_{av} value for Sample A7 reduced by 74%, whereas only 55% for sample A1 .

Insert Figure 5

4.4. Effect of needle punch density

Another very important technic parameter for needle punch nonwoven is the needling density. Similar approach is used here by selecting Samples A1 (50E4 punches/m^2), A2 (130 punches/m^2) and A3 (210 punches/m^2) that are nearly identical in initial sample density ρ_{so}, yet with an increasing needling density. Fig. 6 demonstrates the effect of increasing needling density on the average flow speed v_{av} with varying pressures using data from the 3 samples, where again all the differences shown between the curves are virtually due to the needling density. It is clear that increasing the needling density has a similar effect as either increasing the pressure P or increasing the initial sample density ρ_{so}, all leading to a tighter structure with more fiber entanglement and hence a reduced flow speed v_{av}. This time, the pressure impacts more significantly for a sample with lower needling density. Sample A7 with the lowest needling

density possessed clearly the highest flow speed v_{av} at low pressure, but at high pressure level, the v_{av} values for all 3 specimens reduced to an nearly identical value.

Insert Figure 6

4.5. Performance/Evaluation of Padding

Noting the padding specimens serve two main functions of providing uniform pressure and channeling away body fluids, several inferences can be drawn from this study on the real time performance of padding bandages in fluid management:

1. Padding materials should be made as isotropic as possible, for any anisotropy will lead to behavior variations at different directions, thus causing non-uniform pressure supply and less effective fluid absorption in certain directions. Nonwoven fabrics are hence preferred than woven or knitted ones;
2. Different pressure levels are recommended at different stages of chronic venous disorders, yet the underneath padding will perform differently depending on the applied compression on the limb. When pressure increases, the structure becomes less porous and thus obstructs the liquid movement, causing slower evaporation of the body fluid, and promoting more accumulation of fluid that may cause discomfort to patients. It is therefore recommended to use different padding materials for different pressure levels to ensure the same efficiency in fluid management. A balance should be established between sufficient pressure level and acceptable level of remaining porosity;
3. There are a few other factors including the material initial density and the extend of fiber entanglement (needling density for needle punch nonwovens) which also influence

the liquid flow in the padding. Increasing the sample density or needling density has the similar effect as increasing the pressure, all leading to a denser and less absorbent system;

4. There exists certain interplaying between the related parameters so that performance ranking may reverse in some cases. For instance in Fig. 6, although a low needle punch density sample (A7, 50E4 punches/m^2) shows faster spreading speed v_{av} (0.0171 cm/s) compared to the higher density sample (A9, 210E4 punches/m^2 ,v_{av} = 0.0054 cm/s) at low level of pressure (0.2 kPa;). But, at 2 kPa, the v_{av} for A7, A8 and A9 are nearly identical. This indicates the performance of a product is also a function of the deploying conditions and should be assessed accordingly.
5. In some cases, the padding is also used for lowering the internal pressure at critical regions especially over bony prominences such as tibia or fibula. In general practice, a heavier or thicker padding is recommended in order to obtain maximum pressure reduction. However, a heavier padding will be more obstructive in liquid flow;
6. The results showed that the decrease in either specimen density or needle punch density improves the rate of liquid spreading at a given compression. Several preparatory methods can be employed to optimize the porous network of the padding, for instance, by changing the machine parameters such as laying factor, number of needle stroke, depth of needle penetration etc., in the needle-punching nonwoven machine.

5. Conclusions

The testing apparatus introduced in this study provides a useful and effective tool to study and record the in-plane liquid transport behaviors in porous sheet materials under different

pressure levels. It can obtain several parameters related to the liquid transport simultaneously along different directions in a sample.

The Lucas–Washburn theory describes the capillary-driven nonhomogeneous flows in a cylindrical capillary tube at a given direction. If a comprehensive effective capillary radius r_α can be derived which will generate, at the macro-level, the equivalent kind of flow as in the original porous material, this capillary tube theory can then be applied to deal with the general liquid flow in a porous medium. Furthermore, if one can develop a complete expression r_α in which such related factors as the normal pressure applied, the sample bulk density and the needling density (for nonwovens) can be explicitly included, the theory will be capable of predicting the influence of these factors so as to guide the product design and selection.

Two parameters are developed in this study to describe the flow anisotropy of products, the total travel time T_α at different directions α within a sample, and the overall flow anisotropic index I_A for each sample. Although I_A offers a convenient and comprehensive indicator when comparing between different samples, T_α is more useful and sensitive in describing the specific flow details between different flow directions in the same sample.

Of the three influencing factors discussed, i.e., the normal pressure applied, the sample bulk density and the needling density, increasing either factor will generate similar effect to compacting the sample, thus reducing the effective capillary radius r_α and slowing down the flow speed.

References

1. Zaman HU, Islam JMM, Khan MA, Khan RA. Physico-mechanical properties of wound dressing material and its biomedical application. J Mech Behav Biomed Mater. 2011 Oct;4(7):1369-75. PubMed PMID: WOS:000294187500047. English.

2. Rajendran S, Anand SC. Contribution of textiles to medical and healthcare products and developing innovative medical devices. Indian J Fibre Text. 2006;31(1):215-29.
3. Xu H, Yuan XD, Shen BD, Han J, Lv QY, Dai L, et al. Development of poly(N-isopropylacrylamide)/alginate copolymer hydrogel-grafted fabrics embedding of berberine nanosuspension for the infected wound treatment. Journal of Biomaterials Applications. 2014 May;28(9):1376-85. PubMed PMID: WOS:000334636700009.
4. Nathan M, inventor; Hartford Corporation, assignee. Multilayer absorbent structure. US4360015 A patent US4360015 A. 1982.
5. Partsch H. Compression therapy in leg ulcers. Reviews in Vascular Medicine. 2013;1(1):9-14.
6. Mosti G, Picerni P, Partsch H. Compression stockings with moderate pressure are able to reduce chronic leg oedema. Phlebology. 2012 Sep;27(6):289-96. PubMed PMID: ISI:000312350100003. English.
7. Dale JJ, Ruckley CV, Gibson B, Brown D, Lee AJ, Prescott RJ. Multi-layer compression: comparison of four different four-layer bandage systems applied to the leg. European journal of vascular and endovascular surgery : the official journal of the European Society for Vascular Surgery. 2004 Jan;27(1):94-9. PubMed PMID: 14652845.
8. Moffatt CJ, McCullagh L, O'Connor T, Doherty DC, Hourican C, Stevens J, et al. Randomized trial of four-layer and two-layer bandage systems in the management of chronic venous ulceration. Wound repair and regeneration : official publication of the Wound Healing Society [and] the European Tissue Repair Society. 2003 May-Jun;11(3):166-71. PubMed PMID: 12753596.
9. Fauland G, Lenz A, Rohrer C, Bechtold T. Assessment of moisture management performance of multilayer compression bandages. Text Res J. 2012;83(8):871-80.
10. Kumar B, Das A, Alagirusamy R. Effect of material and structure of compression bandage on interface pressure variation over time. Phlebology. 2013;29(6):376-85. Pubmed Central PMCID: 23571751.
11. Rossi RM, Stämpfli R, Psikuta A, Rechsteiner I, Brühwiler PA. Transplanar and in-plane Wicking Effects in Sock Materials Under Pressure. Text Res J. 2011;81(15):1549-58.
12. Cutting KF, White RJ. Avoidance and management of peri-wound maceration of the skin. Professional nurse. 2002 Sep;18(1):33, 5-6. PubMed PMID: 12238719.
13. Midha VK, Mukhopadyay A. Bulk and physical properties of needle-punched nonwoven fabrics. Indian J Fibre Text. 2005 Jun;30(2):218-29. PubMed PMID: WOS:000230542900018.
14. Pan N, Zhong W. Fluid Transport Phenomena in Fibrous Materials. Textile Progress. 2006;38(2):1-93.
15. Kumar B, Das A, Alagirusamy R. Prediction of internal pressure profile of compression bandages using stress relaxation parameters. Biorheology. 2012;49(1):1-13. PubMed PMID: ISI:000305435900001. English.
16. Farah RS, Davis MDP. Venous Leg Ulcerations:A Treatment Update. Current Treatment Options in Cardiovascular Medicine. 2010;12:101-16.
17. Mhetre S, Parachuru R. The effect of fabric structure and yarn-to-yarn liquid migration on liquid transport in fabrics. Journal of the Textile Institute. 2010;101(7):621-6. PubMed PMID: ISI:000278924800004. English.
18. Kissa E. Wetting and wicking. Text Res J. 1996 Oct;66(10):660-8. PubMed PMID: ISI:A1996VK97000009. English.

19. Lukas D, Soukupova V, Pan N, Parikh DV. Computer simulation of 3-D liquid transport in fibrous materials. Simulation-Transactions of the Society for Modeling and Simulation International. 2004 Nov;80(11):547-57. PubMed PMID: WOS:000227293500001.
20. Zhu L, Perwuelz A, Lewandowski M, Campagne C. Static and dynamic aspects of liquid capillary flow in thermally bonded polyester nonwoven fabrics. J Adhes Sci Technol. 2008;22(7):745-60. PubMed PMID: ISI:000257949700006. English.
21. Raja D, Ramakrishnan G, Babu VR, Senthilkumar M, Sampath MB. Comparison of different methods to measure the transverse wicking behaviour of fabrics. J Ind Text. 2014 Jan;43(3):366-82. PubMed PMID: ISI:000328607900005. English.
22. Babu VR, Koushik CV, Lakshmikantha CB, Subramaniam V. Capillary rise in woven fabrics by electrical principle. Indian J Fibre Text. 2011 Mar;36(1):99-102. PubMed PMID: ISI:000289823400014. English.
23. Kumar B, Das A, Alagirusamy R, Singh J, Garg V, Gupta R. Characterization of liquid transport in needle-punched nonwovens. I. Wicking under infinite liquid reservoir. Fibers and Polymers. 2014;15(12):2665-70.
24. Ansari N, Kish MH. The wicking of water in yarn as measured by an electrical resistance technique. Journal of the Textile Institute. 2000;91(3):410-9. PubMed PMID: ISI:000168805800006. English.
25. Ito H, Muraoka Y. Water Transport Along Textile Fibers as Measured by an Electrical Capacitance Technique. Text Res J. 1993 Jul;63(7):414-20. PubMed PMID: ISI:A1993LK54900006. English.
26. Kumar B, Das A. Vertical Wicking Behavior of Knitted Fabrics. Fibers and Polymers. 2014;15(3):625-31.
27. Kumar B, Das A. Design and development of a Computerized Wicking Tester for longitudinal wicking in fibrous assemblies. Journal of the Textile Institute. 2014;105(8):850-9.

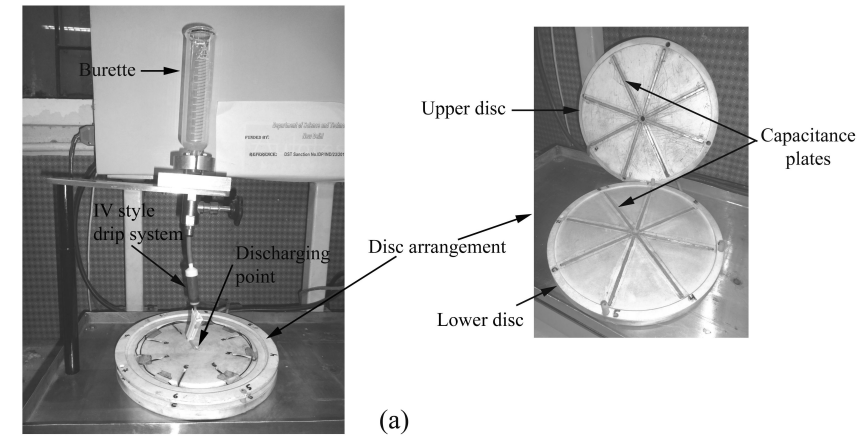

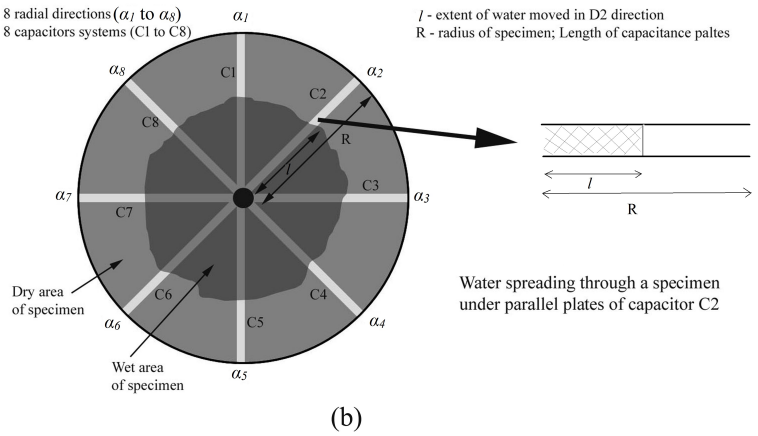

Fig. 1. (a) Photograph of the instrumental set-up for measuring wicking process; (b) Schematic of the liquid flow through an arc padding specimen placed between the parallel plates of capacitor systems.

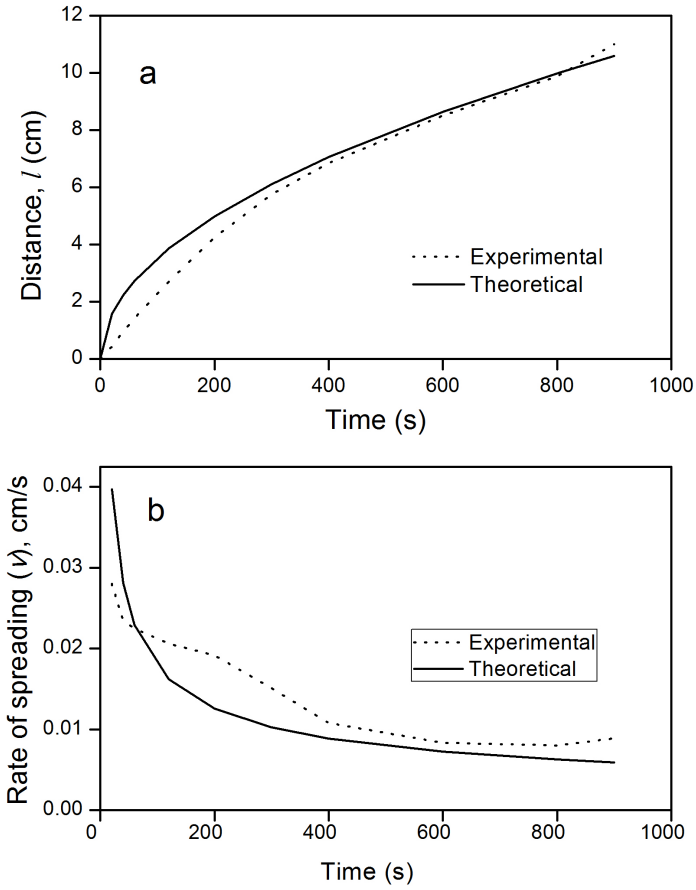

Fig. 2. For sample A2 at direction α_1, P =0.2 kPa: (a) Wicking length vs time; (b) Rate of spreading vs time.

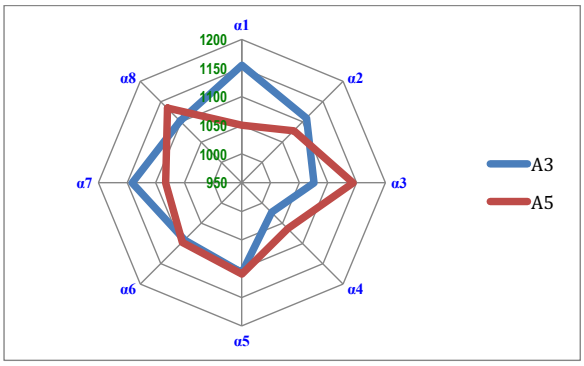

Fig. 3: Comparison between Samples A3 and A5

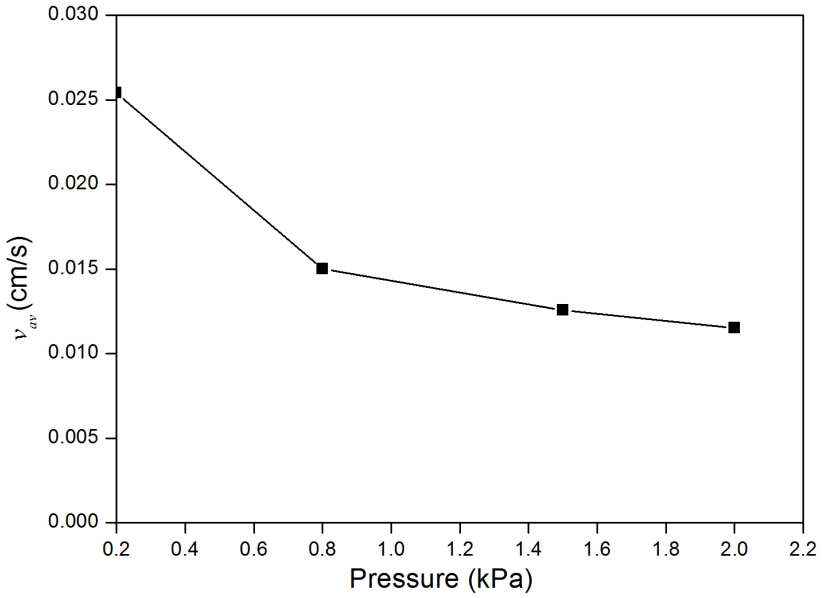

Fig. 4. Experimental results of maximum liquid spreading rate at different levels of normal pressure (Sample A1).

Deleted: and predicted

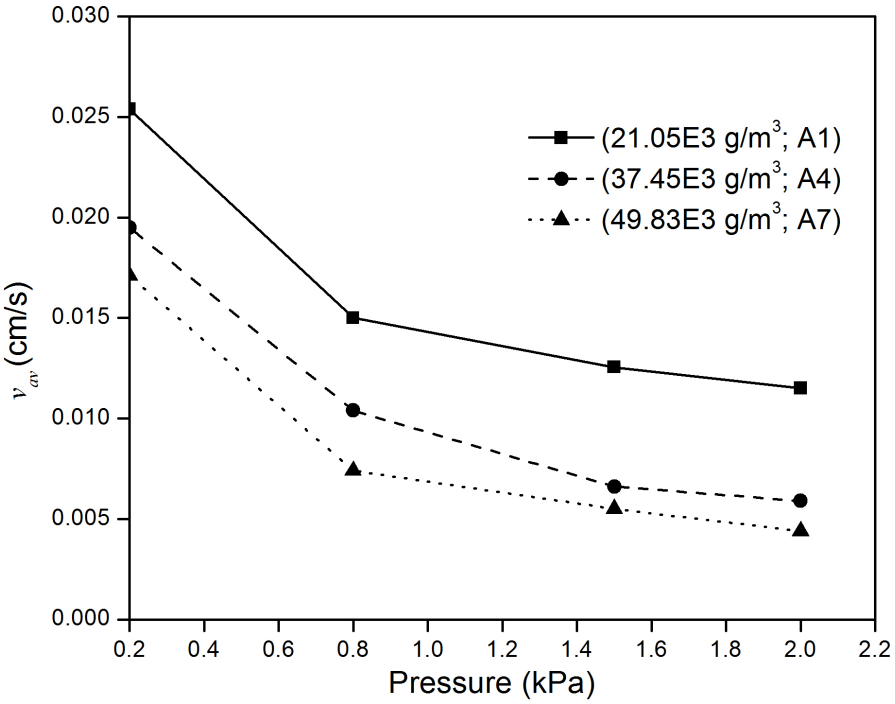

Fig. 5. Effect of sample initial density on the flow spreading rate.

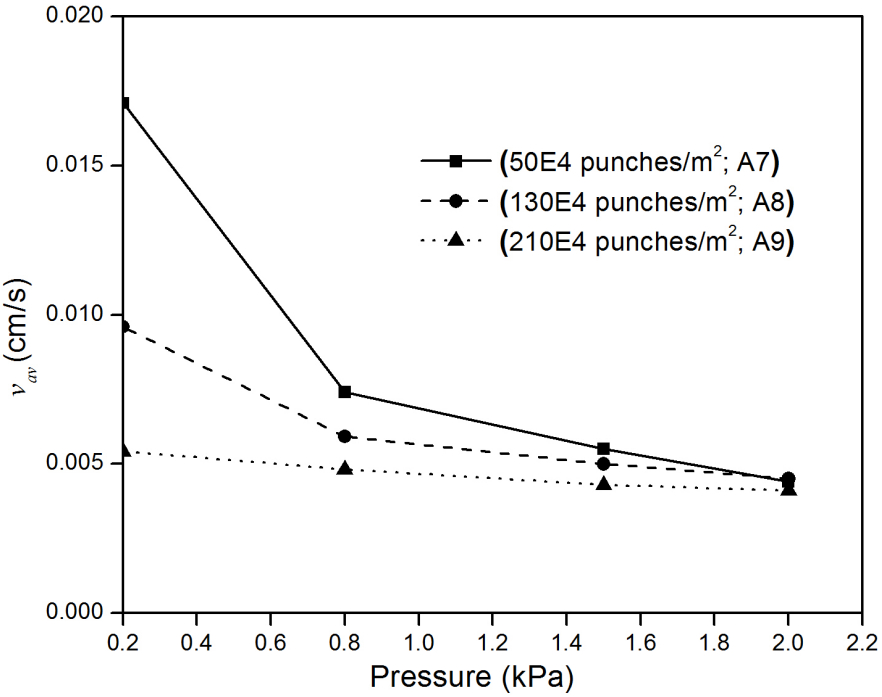

Fig. 6. Effect of needle density on v_{av} with increasing pressure.